NiO-polyoxometalate nanocomposites as efficient catalysts for the oxidative dehydrogenation of propane and isobutane

Qinghong Zhang, Chuanjing Cao, Ting Xu, Miao Sun, Jizhe Zhang, Ye Wang* and Huilin Wan*

Electronic Supplementary Information

1. Experimental details

(1) Preparation of the NiO-POM composites

The NiO-POM composites with different compositions were prepared by a citric acid complexation method using $Ni(NO_3)_2$, Cs_2CO_3 and $H_3PMo_{12}O_{40}$ as the starting materials. Typically, $Ni(NO_3)_2{\cdot}6H_2O$ was first dissolved into a citric acid aqueous solution, and the molar ratio of citric acid to Ni^{2+} was kept at 1/1. Then, Cs_2CO_3 aqueous solution was added with stirring, and a green mixed solution was obtained. The mixed solution was kept at 70 ^oC for 30 min under vigorous stirring to ensure the complexation of citric acid with both Ni^{2+} and Cs^+ cations. After that, an aqueous solution of $H_3PMo_{12}O_{40}$ was added, and the molar ratio of Cs^+ to $PMo_{12}O_{40}^{3-}$ was fixed at 2.5. A suspension was obtained because of the interaction of $PMo_{12}O_{40}^{3-}$ with Cs^+. The suspension was further kept under continuous stirring until it became a gel. The gel was dried at 120 ^oC for 24 h, and subsequently calcined in air at 500 ^oC for 4 h. Single NiO and $Cs_{2.5}H_{0.5}PMo_{12}O_{40}$ were also prepared using the same procedure.

(2) Characterization of NiO-POM composites

XRD, N_2 sorption, SEM, TEM, XPS, NH_3-TPD and O_2-TPD were used to characterize the structures and the adsorption properties of the NiO-POM composites. XRD patterns were recorded on a Panalytical X'Pert Pro Super X-ray diffractometer equipped with X'Celerator detection system. Cu-K_α radiation (40 kV and 30 mA) was used as the X-ray source. N_2 sorption at -196 ^oC was carried out with a Micromeritics Tristar 3000 surface and porosimetry analyzer. SEM was done using a LEO1530 scanning electron microscope with 20 kV accelerating voltage. TEM measurements were performed on a Tecnai F30 electron microscope (Phillips Analytical) operated at an acceleration voltage of 300 kV. Samples for TEM measurements were suspended in ethanol and dispersed ultrasonically. Drops of the suspensions were applied on a copper grid coated with carbon. NH_3-TPD and O_2-TPD were performed using a Micromeritics AutoChem II 2920 instrument connected to a ThermoStar GSD 301 T2 mass spectrometer.

(3) Catalytic reaction

The catalytic reactions were carried out using a fixed-bed quartz reactor (i.d., 10 mm) operated at atmospheric pressure. The products were analyzed by two on-line gas chromatographs.

2. EDS analysis for the 80% NiO-POM nanocomposite

Fig. S1 shows the EDS analysis (mapping) results for the 80% NiO-POM nanocomposite. It can be seen from Fig. S1 that all the elements are homogeneously distributed in the sample.

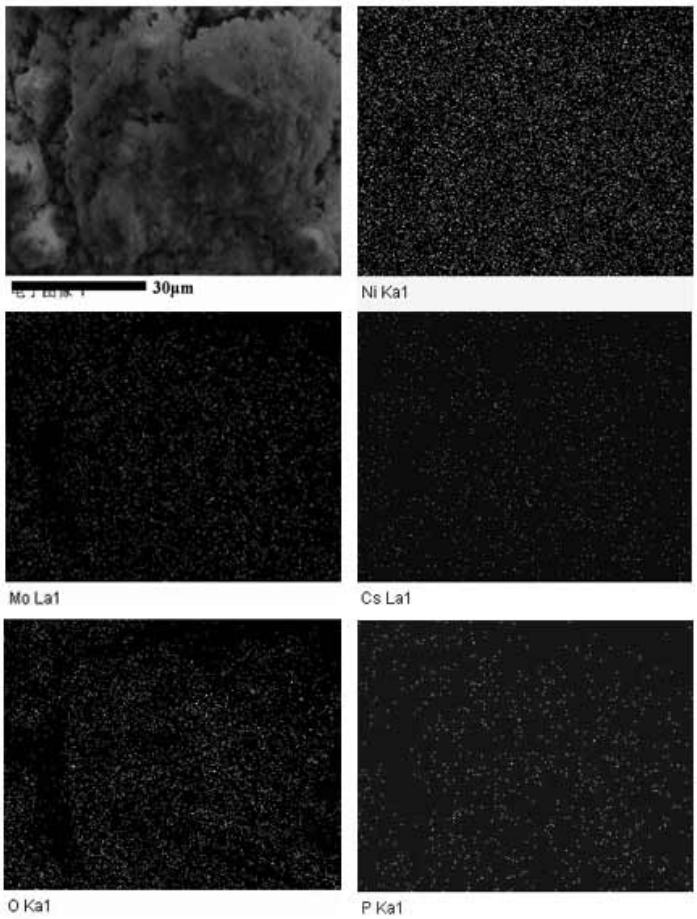

Fig. S1 SEM image and corresponding EDS elemental analysis (mapping) for the 80% NiO-POM.

3. BET surface areas of the NiO-POM nanocomposites together with single NiO and POM

Table S1 BET surface areas of the NiO-POM nanocomposites together with single NiO and POM

Sample	Surface area (m^2/g)
NiO	20
85% NiO-POM	137
80% NiO-POM	138
75% NiO-POM	118
70% NiO-POM	108
50% NiO-POM	43
30% NiO-POM	21
POM ($Cs_{2.5}H_{0.5}PMo_{12}O_{40}$)	90

4. Adsorption amounts of O_2 and NH_3 over the NiO-POM nanocomposites evaluated from the O_2- and NH_3-TPD measurements

Table S2 shows the adsorption amounts of O_2 and NH_3 over the NiO-POM nanocomposites evaluated from Fig. 4. The intensities of mass signals were calibrated by using fixed amounts of NH_3 and O_2 as references. The NiO-POM composites containing 80-85 wt% NiO showed higher O_2 adsorption amount per gram of sample than single NiO. The adsorption amount of O_2 per surface area for these samples became lower than that for NiO. For the nanocomposites containing 30-75 wt% NiO and the single POM, the adsorption amounts of O_2 became significantly lower. These results tend to suggest that the O_2 adsorption ability comes from the surface NiO over the nanocomposites.

On the other hand, the NiO-POM nanocomposites showed significantly higher amounts of NH_3 adsorption (either per gram of sample or per surface area) as compared to single NiO or single POM, and the maximum adsorption amount of NH_3 was observed over the 75% NiO-POM nanocomposite.

Table S2 Adsorption amounts of O_2 and NH_3 over the NiO-POM nanocomposites evaluated from the O_2- and NH_3-TPD measurements

Sample	O_2 (μmol/g)	O_2 (μmol/m^2)	NH_3 (μmol/g)	NH_3 (μmol/m^2)
NiO	20	1	0	0
85% NiO-POM	27	0.20	120	0.88
80% NiO-POM	23	0.17	150	1.1
75% NiO-POM	13	0.11	160	1.4
70% NiO-POM	7	0.06	140	1.3
50% NiO-POM	5	0.11	40	0.93
30% NiO-POM	0	0	10	0.48
POM ($Cs_{2.5}H_{0.5}PMo_{12}O_{40}$)	0.5	0.01	20	0.22

5. FT-IR spectra of adsorbed NH_3 on NiO-POM nanocomposites together with single compounds

Fig. S2 shows the FT-IR spectra of adsorbed NH_3 on NiO-POM nanocomposites together with NiO and POM ($Cs_{2.5}H_{0.5}PMo_{12}O_{40}$). The POM exhibited an IR band at 1450 cm^{-1}, assignable to NH_3 adsorbed on Brønsted acid sites (D. Robert, T. Didier, *J. Phys. Chem. B*, 2000, **104**, 11117), whereas IR bands for single NiO were very weak. The NiO-POM nanocomposites showed IR bands at 1610 and 1220 cm^{-1}, which could be ascribed to NH_3 adsorbed on Lewis acid sites (D. Robert, T. Didier, *J. Phys. Chem. B*, 2000, **104**, 11117). Therefore, the acidic sites over the NiO-POM nanocomposites were mainly the Lewis type in nature.

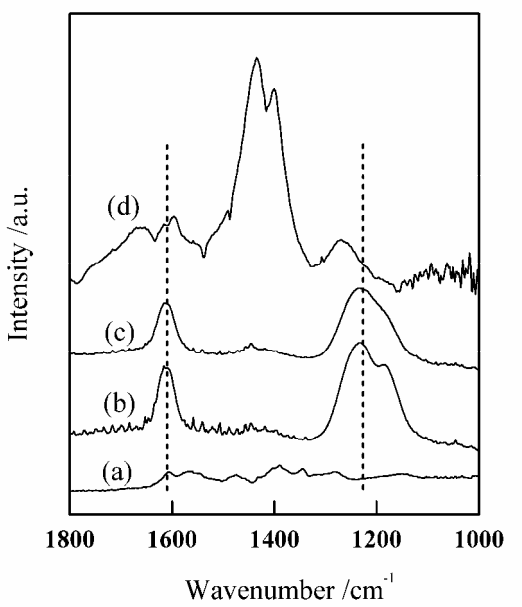

Fig. S2 FT-IR spectra of ammonia adsorbed on different samples (a) NiO, (b) 80% NiO-POM, (c) 70% NiO-POM, (d) POM.

6. Plots of propene selectivity versus propane conversion over NiO and the 80% NiO-POM catalysts

Fig. S3 shows the plots of propene selectivity versus propane conversion over NiO and the 80% NiO-POM nanocomposite. It is clear that the 80% NiO-POM is a more selective catalyst for the ODH of propane.

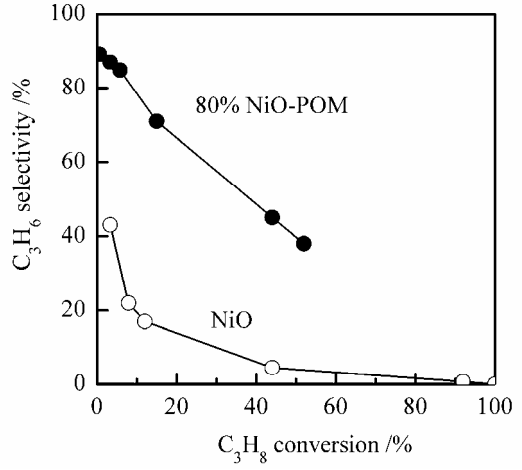

Fig. S3 Propene selectivity versus propane conversion over NiO and the 80% NiO-POM composite. Reaction conditions: W = 0.50 g; T = 250-500 °C; $P(C_3H_8)$ = 4.1 kPa; $P(O_2)$ = 16.2 kPa; $P(N_2)$ = 81.1 kPa; F(total) = 50 mL min^{-1}.

7. Stability of the 80% NiO-POM nanocomposite in the ODH of propane

Fig. S4 shows the change of catalytic performances with time on stream over the 80%

NiO-POM nanocomposites for the ODH of propane.

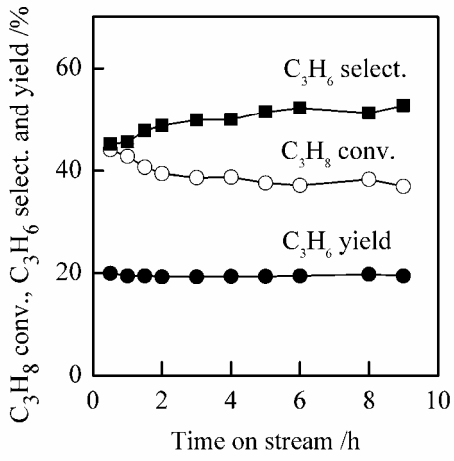

Fig. S4 Change of catalytic performances with time on stream over the 80% NiO-POM for the ODH of propane. Reaction conditions: W = 0.50 g; T = 450 ^{o}C; $P(C_3H_8)$ = 4.1 kPa; $P(O_2)$ = 16.2 kPa; $P(N_2)$ = 81.1 kPa; F(total) = 50 mL min^{-1}.

8. FT-IR spectra of the NiO-POM nanocomposites before and after catalytic reactions

Fig. S5 shows the FT-IR spectra of the NiO-POM nanocomposites before and after catalytic reactions (propane oxidative dehydrogenation under conditions of Table 1). The single $Cs_{2.5}H_{0.5}PMo_{12}O_{40}$ (Fig. S6A) before reaction but after calcination at 500 ^{o}C exhibited a typical vibration pattern of Keggin-type molybdophosphate anion ($PMo_{12}O_{40}^{3-}$). The observed IR bands at 1062, 964, 867 and 796 cm^{-1} could be attributed to the asymmetric stretching of the central atom-oxygen (P–O) bond of PO_4 tetrahedron, the asymmetric stretching of peripheral atom-terminal oxygen (Mo=O) bond and the Mo–O–Mo oscillations of the inter- and intra-octahedral bridges of trimetallic group, respectively (T. Okuhara, N. Mizuno and M. Misono, *Adv. Catal.* 1996, **41**, 113). Moreover, for $Cs_{2.5}H_{0.5}PMo_{12}O_{40}$ alone, no significant changes in IR spectrum were observed after catalytic reactions (Fig. S6B), suggesting that the Keggin structure of $Cs_{2.5}H_{0.5}PMo_{12}O_{40}$ was stable after calcination at 500 ^{o}C and after further catalytic reactions at 450 ^{o}C.

For the NiO-POM nanocomposites, a set of four IR bands similar to those of POM could be observed although the intensities of these bands were reduced. The positions of the bands attributable to the terminal oxygen (Mo=O) bond and the Mo–O–Mo oscillations shifted to some extent. We suggest that the POM structure in the NiO-POM nanocomposites may be distorted to some extent. A new band at ~713 cm^{-1} might be ascribed to the newly formed Mo-O-Ni bond in the nanocomposites. For the nanocomposites, no significant changes in FT-TR spectra could be detected after the catalytic reaction. Therefore, the structure of the NiO-POM nanocomposites was stable during the catalytic reaction.

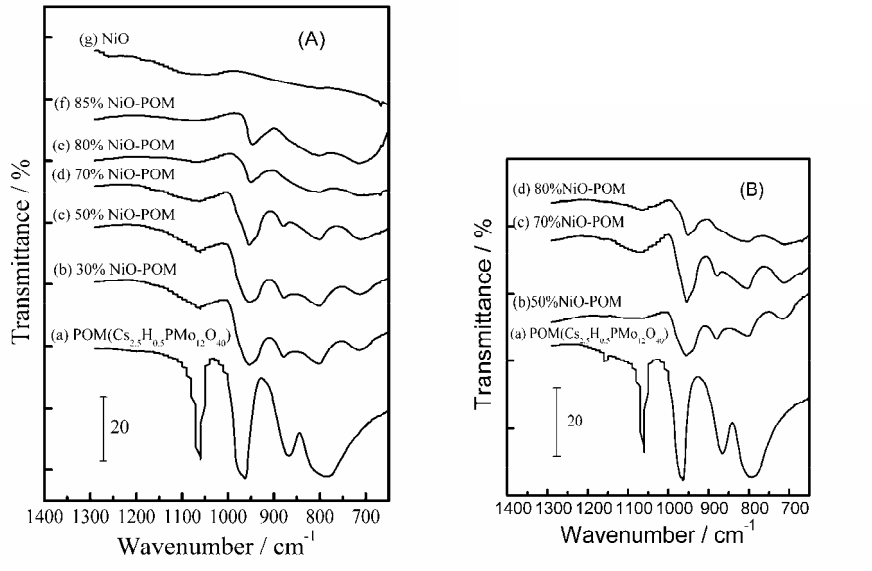

Fig. S5 FT-IR spectra of the NiO-POM composites together with single NiO and $Cs_{2.5}H_{0.5}PMo_{12}O_{40}$. (A) Before catalytic reactions; (B) after catalytic reactions.

9. Stability of the 70% NiO-POM nanocomposite in the ODH of isobutane

Fig. S6 shows the change of catalytic performances with time on stream over the 70% NiO-POM for the ODH of isobutane.

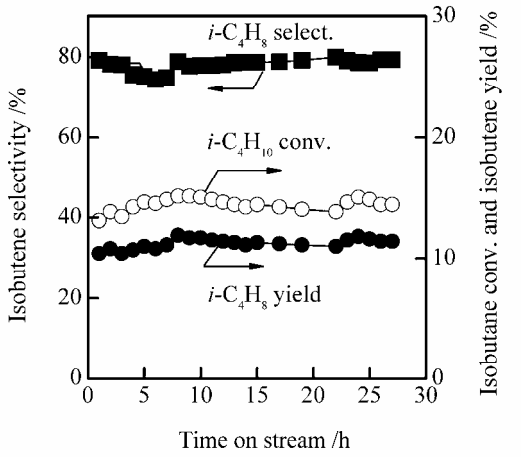

Fig. S6 Change of catalytic performances with time on stream over the 80% NiO-POM for the ODH of isobutane. Reaction conditions: W = 0.50 g; T = 450 °C; $P(i\text{-}C_4H_{10})$ = 5.6 kPa; $P(O_2)$ = 11.2 kPa; $P(N_2)$ = 84.2 kPa; F(total) = 90 mL min^{-1}.